4-17-2004

Upper Mantle P-Wave Velocity Structure from Passcal Teleseismic Transects Across Idaho, Wyoming and Colorado

Ken Dueker
University of Wyoming, dueker@uwyo.edu

H. Y. Yuan

Publication Information

Dueker, Ken and Yuan, H. Y. (2004). "Upper Mantle P-Wave Velocity Structure from Passcal Teleseismic Transects Across Idaho, Wyoming and Colorado." *Geophysical Research Letters* 31.8.

Upper mantle P-wave velocity structure from PASSCAL teleseismic transects across Idaho, Wyoming and Colorado

Ken Dueker and Huaiyu Yuan

Department of Geology and Geophysics, University of Wyoming, Laramie, Wyoming, USA

Received 12 January 2004; revised 10 March 2004; accepted 19 March 2004; published 17 April 2004.

[1] Inversion of teleseismic P-time residuals along two linear seismic arrays provides well-resolved inverse images of the upper mantle. Low velocity bodies beneath the Yellowstone Hotspot Track and the Grand Mesa volcanic field in western Colorado are similar in shape and magnitude. In the two places where our transects cross the 1.78 Ga Archean-Proterozoic Cheyenne suture, high velocities are imaged to 150 km. Beneath the Leucite Hills volcanic field in Wyoming a small upper mantle low velocity body is imaged. Whether these anomalies are lithospheric or asthenospheric in origin is poorly constrained, but the consistent high velocities beneath the Cheyenne suture suggest a lithospheric origin. Likewise, the lack of extension beneath the western Colorado volcanic fields suggests that a low-solidus lithosphere is being disturbed by a regional heating event. *INDEX TERMS:* 7218 Seismology: Lithosphere and upper mantle; 8110 Tectonophysics: Continental tectonics—general (0905); 8120 Tectonophysics: Dynamics of lithosphere and mantle—general. **Citation:** Dueker, K., and H. Yuan (2004), Upper mantle P-wave velocity structure from PASSCAL teleseismic transects across Idaho, Wyoming and Colorado, *Geophys. Res. Lett.*, *31*, L08603, doi:10.1029/2004GL019476.

1. Introduction

[2] Previous teleseismic P- and S-wave velocity images show that velocity heterogeneity beneath the intermountain western United States is pervasive and large (8% δV_p) above 200 km depth [*Dueker et al.*, 2001; *Gao et al.*, 2004; *Humphreys et al.*, 2003; *Lee and Grand*, 1996; *Schutt and Humphreys*, 2004; *Yuan and Dueker*, 2004]. The most resolved images show sharp lateral velocity variations (6–8% δV_p over 50–100 km) that are sometimes separated by a dipping boundary [*Gök et al.*, 2003; *Yuan and Dueker*, 2004]. The association of these velocity contrasts with sutures suggests that these anomalies are, at least partly, lithospheric in origin [*Dueker et al.*, 2001; *Karlstrom and CDROM Working Group*, 2002]. In cases where a low velocity body underlies a suture, we suggest that low-solidus materials (e.g., hydrated rocks, sediments, eclogite) may be preferentially melting during regional heating events. In addition, sutures likely contain strength and density contrasts that may localize lithospheric thermal instabilities [*Schott et al.*, 2000] and provide focused heat exchange between the lithosphere and underlying mantle. In contrast, where a dipping high velocity body has been imaged beneath the Cheyenne belt suture, we suggest an ancient slab was trapped during the 1.7 Ga accretionary process [*Yuan and Dueker*, 2004].

[3] Constraining the dynamical origin of upper mantle velocity heterogeneity continues to be a difficult endeavor due to several factors. First, the station distribution is often rather sparse (>20 km station spacing) resulting in inverse images whose resolution is strongly conditioned by the regularization used. Second, when crustal thickness variations are large and deep sedimentary basins are present, accurate crustal travel-time corrections are required. Third, the travel-time effect of velocity anisotropy will create artifacts in isotropic inverse images [*Granet et al.*, 1988; *Yuan and Dueker*, 2004]. Fourth, the conversion of velocity perturbations into a thermal field requires accurate 3-D model of attenuation [*Sobolev et al.*, 1997] and melt can significantly perturb the velocity [*Goes and van der Lee*, 2002]. In this study, the first two concerns have been overcome given our 12 km station spacing and coincident receiver function images [*Crosswhite and Humphreys*, 2003] and active source studies [*Henstock et al.*, 1998; *Snelson et al.*, 1998]. However, the influence of anisotropy is poorly constrained due to the poor SKS sampling provided by our short deployments and only regional attenuation (Q) models exist for this region.

2. Data and Methods

[4] Our data set is formed from three teleseismic transects (Figure 1): the five month 1993 Snake River Plains (SRP-93) transect, the three month 1997 Deep Probe N-S transect (DP-NS) and the three month 1997 Deep Probe NW-SE transect (DP-NW). The DP-NW transect was deployed to purposely overlap with the SRP-93 line and these two transects data are combined to produce the 1000 km long Snake River Plain-Deep Probe (SRP-DP) transect. The teleseismic P-wave relative residuals for direct-P, PcP, and PKiKP phases have been measured using multi-channel cross correlation [*Vandecar and Crossen*, 1990]. To improve error estimates and equalize resolution, a summary ray data set is formed by mapping the P-residuals for each station onto a slowness grid. The summary ray value and standard error at each grid point is calculated as a Guassian weighted average where the half-width of the Guassian is 0.015 s/km. To account for the travel-time effects of basins and crustal thickness variations, teleseismic P-wave corrections have been calculated from the coincident receiver function studies [*Crosswhite and Humphreys*, 2003; *Peng and Humphreys*, 1998], the basin thickness estimate from the Deep Probe refraction results [*Snelson et al.*, 1998] and published depth to basements maps. The RMS of the crustal corrections for the SRP-DP and DP-NS lines are 0.07 s and

0094-8276/04/2004GL019476

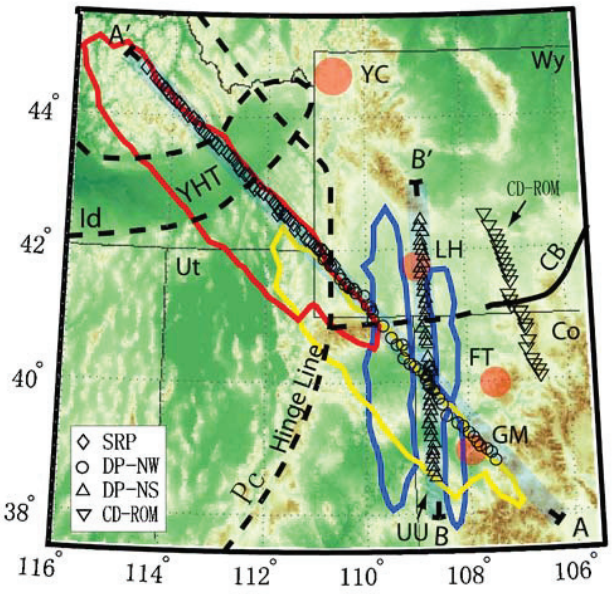

Figure 1. PASSCAL seismic stations, ray sampling and topography. The red, blue and yellow lines contour the ray density for the three arrays at 200 km depth. Volcanic and geologic features denoted as: CB, Cheyenne belt suture; YHT, Yellowstone Hotspot Track; YC, Yellowstone Caldera; UU, Uncompahgre Uplift; GM, Grand Mesa volcanic field; FT, Flat Tops volcanic field; LH, Leucite Hills volcanic field. Cross sections for the Snake River Plain/Deep Probe transect (A-A′) and Deep Probe N-S (B-B′) are marked.

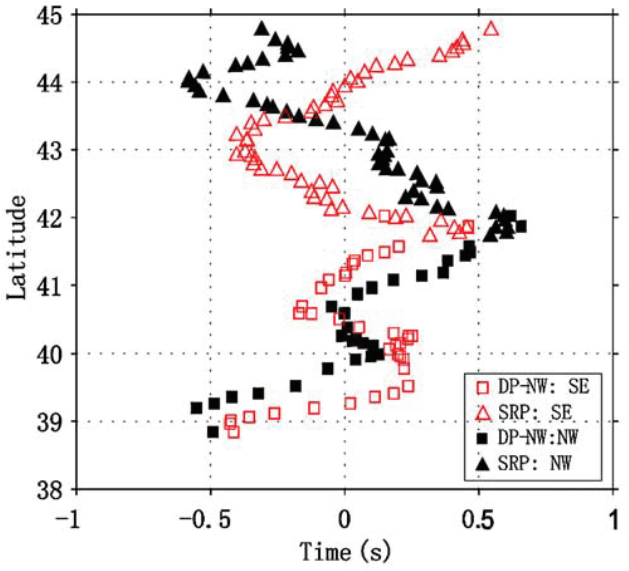

Figure 2. Teleseismic P-wave summary-ray residuals for the Deep Probe-Snake River Plain (DP-SRP) transect. Negative and positive residuals are late and early arrivals, respectively. Note that where the two arrays meet at 41.9°, the residuals from both back-azimuths are consistent, implying that any possible baseline shift between the two different relative residual data sets is insignificant.

0.09 s, respectively. Figure 2 shows that that the summary ray residuals for the SRP93 and DP-NW data sets match up very well where the two arrays meet.

[5] The model space is parameterized as a two-dimensional grid of constant slowness blocks that are 15 km wide and 20 km in depth. To account for the minor effects of the Earth's sphericity on the upper 200 km of our model, an Earth flattening transformation is applied to our radial background velocity model. To test for an optimal model depth, a sequence of inversions that varied the model depth between 100–600 km depth were analyzed. This analysis showed that the velocity structure above 200 km remains constant in spatial extent and magnitude for model depths greater than 350 km depth. A linear inversion of the tomographic system of equations is accomplished via matrix inversion of the least squares normal equations. Non-linear inversion, to account for ray bending effects, has not been done because previous work with the SRP-93 portion of our data set shows its effects are minor [*Saltzer and Humphreys*, 1997].

[6] The row space of the data kernel matrix was weighted by the a priori data covariance matrix constructed using the summary ray errors. Note that the summary ray errors are conservative error estimates and are about twice the errors calculated from the cross correlation inversion. Regularization has been applied by weighting the column space of the data kernel matrix with an apriori model covariance matrix and the addition of diagonal damping. Choice of an optimal regularization parameter was found by assessing the trade-off curve between resolution and variance. The damping parameters used result in 81–85% variance reductions with Chi-squared values that slightly underfit the data (Table 1).

3. Results

[7] Our P-wave images show that 8% peak-to-peak velocity variations are pervasive above 150 km depth (Figure 3). Below 150 km, the maximum velocity variation is <3%. The model parameter standard deviations (not standard errors) were calculated using summary ray errors and the error maps (Figures 3c and 3d) show that the model standard deviations are <1%. The spatial resolution of the inversions is assessed via the resolution kernels (Figures 3e and 3f) that reveal excellent resolution. The contour of the ray density at 200 km depth (Figure 1) shows that the SRP-DP line array samples a 120 wide swath to the southwest of the array while the DP-NS line array samples a larger 180 km wide swath. These small sampling footprints in conjunction with the high variance reduction of the models (Table 1) suggests that our 2-D velocity images are not significantly biased by 3-D structure.

Table 1. Data Sets Characteristics

	Raw Data		Summary Ray Data			
Data Set	No. of Residuals	RMS	No. of Residuals	RMS	Variance Reduction (%)	Chi-Square
DP-NS	1484	0.25	1203	0.21	85.68	13.17
DP-NW	1552	0.33	1238	0.28		
SRP	4396	0.38	3239	0.29		
DP-SRP	5948	0.37	4395	0.29	80.72	19.95

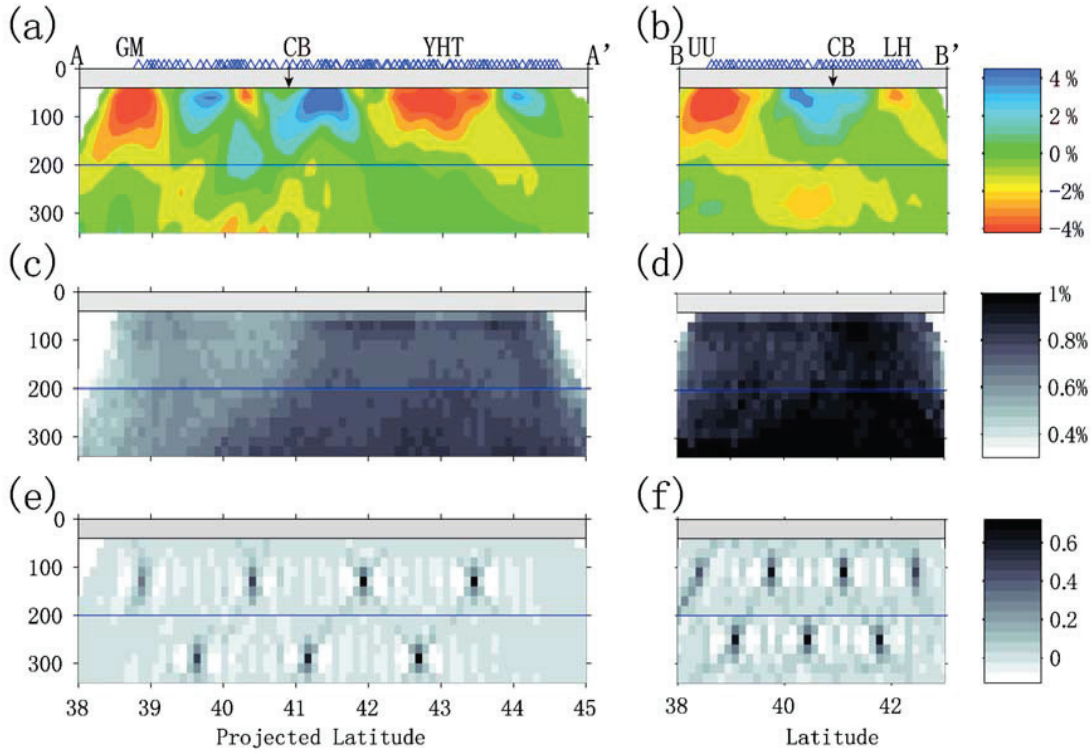

Figure 3. P-wave images. The left-hand column (a, c, e) shows results for the DP-SRP transect and the right-hand column (b, d, f) presents results for the DP-NS transect. The topmost row (a, b) shows the P-wave velocity perturbations. The 8% velocity variation represented by the color pallet is not saturated as the peak to peak velocity variation is 9.2%. The middle row (c, d) shows the standard deviation (not standard error) of the model parameters. The bottom row (e, f) shows the resolution kernels for selected model parameters. The labels are denoted in Figure 1.

[8] The primary velocity anomalies observed along the SRP-DP transect (Figure 3a) are two low velocity bodies beneath the Yellowstone hotspot track (YHT) and the Grand Mesa volcanic field (GMVF) and a high velocity body beneath the Cheyenne belt suture. The velocity anomaly beneath the YHT is consistent with the previous P-wave images produced from the SRP-93 data set [*Saltzer and Humphreys*, 1997; *Schutt and Humphreys*, 2004], except that depth extent of the high velocity anomaly to the SE of the eastern Snake River Plain (i.e., the Cheyenne Belt anomaly) has been resolved to lie above 200 km. The Cheyenne belt high velocity anomaly is observed as a 100 km wide zone that resides slightly north of the inferred location of the Cheyenne belt suture [*Karlstrom and CDROM Working Group*, 2002]. At the southernmost end of this transect, a low velocity body as slow as the YHT body is observed beneath the 12 ma GMFV. While this anomaly is at the edge of our model domain, the travel-times, from both back-azimuth quadrants, are as late as those measured beneath the YHT (Figure 2).

[9] The primary anomaly beneath the N-S Deep Probe line (Figure 3b) is a low velocity body beneath the Uncompahgre uplift. Given the overlap in sampling at the south end of both arrays (Figure 1), this anomaly is best considered as part of the same anomaly imaged beneath the GMVF. Volcanic activity here consists of only one very small volcanic field [*Leat et al.*, 1989]. The transition between low and high velocities is imaged as a 45° south dipping boundary extending to 100 km. Just to the south of the Cheyenne belt suture, a 140 km wide high velocity anomaly extends to 100 km depth. The anomaly possesses its greatest magnitude on the south side which gives the appearance of a northward dip. Beneath the <1 Ma Leucite Hills volcanic field [*Lange et al.*, 2000], a small velocity anomaly is observed between 40–70 km depth.

4. Discussion

[10] Our most important result is that the low velocity anomalies beneath the12 ma volcanic fields of western Colorado [*Leat et al.*, 1989] are very similar in magnitude, volume and depth extent as the YHT anomaly. This is surprising because the volcanic output of the western Colorado fields is very small with respect to the YHT volcanism. Thus, the velocity anomalies are not proportional to magmatic output suggesting that the dominant control on volcanic output is the differing strain regimes between the YHT (few mm/yr of extension [*Humphreys et al.*, 2000]) versus western Colorado (no evidence for extension). To estimate the possible thermal variations mapped by our images, the Intermountain western U.S. Q_s value of 50 [*Al-Khatib and Mitchell*, 1991] is inserted into the anelastic velocity-temperature relation. This shows that our 8% peak to peak V_p anomaly would require a 400° thermal anomaly. In the volcanically active low velocity regions, an equilibrium upper mantle melt

porosity of 0.5–1.0% [*McKenzie*, 1989] may exist; this porosity would cause a 1–4% V_p reduction depending on the assumed melt topology distribution [e.g., *Schmeling*, 1985; *Hammond and Humphreys*, 2000]. Subtracting this potential melt-velocity effect would reduce the required thermal anomaly to 200–350°. Two end-member models capable of producing such thermal variations between the Moho and 200 km, would be: small late-Cenozoic mantle plumes have risen beneath Yellowstone and western Colorado and greatly invaded the lithosphere; or, low solidus "suture" lithosphere has been heated and preferentially melted due to Laramide aged hydration that may have weakening the lower lithosphere and hence promoted subsequent convective destabilization of the lithosphere.

[11] Constraining the origin of these velocity anomalies will require a firm consensus with respect to the post-Laramide uplift history of the southern Rocky Mountains. We believe that the evidence for late Cenozoic uplift of this region (i.e., the southern Rocky Mountains and Colorado Plateau) is compelling enough [*Karlstrom and CDROM Working Group*, 2002; *McMillan et al.*, 2002; *Sahagian et al.*, 2002] to suggest that a regional lithospheric reheating event is occurring. This increased heat flux could be driven by a poorly constrained combination of convective removal of the lower lithosphere and/or increased mantle heat flux from small plumes. Beneath the Jemez volcanic lineament, the occurrence of strong sub-crustal velocity layering within the Jemez low velocity upper mantle body has been interpreted to manifest low solidus suture lithosphere being perturbed by a regional heating event [*Zurek and Dueker*, 2004]. Finally, the high velocity bodies imaged beneath the Cheyenne belt on both transects is consistent with the CD-ROM velocity images 250 km to the east of our new transects (Figure 1). This suggest that a casual relationship between the high-velocity anomaly and the Cheyenne belt suture is robust [*Yuan and Dueker*, 2004; *Zurek and Dueker*, 2004].

[12] **Acknowledgments.** We thank the IRIS PASSCAL facility for the seismic equipment and the NSF Continental Dynamics program for funding.

References

Al-Khatib, H. H., and B. J. Mitchell (1991), Upper mantle anelasticity and tectonic evolution of the western United States from surface wave attenuation, *J. Geophys. Res.*, *96*, 18,129–18,146.

Crosswhite, J. A., and E. D. Humphreys (2003), Imaging the mountainless root of the 1.8 Ga Cheyenne belt suture and clues to its tectonic stability, *Geology*, *31*(8), 669–672.

Dueker, K., H. Yuan, and B. Zurek (2001), Thick-structured Proterozoic lithosphere of the Rocky Mountain region, *GSA Today*, *11*(12), 4–9.

Gao, W., S. Grand, S. Baldridge, et al. (2004), Upper mantle convection beneath the central Rio Grande rift imaged by P and S wave tomography, *J. Geophys. Res.*, *109*, B03305, doi:10.1029/2003JB002743.

Goes, S., and S. van der Lee (2002), Thermal structure of the North American uppermost mantle inferred from seismic tomography, *J. Geophys. Res.*, *107*(B3), 2050, doi:10.1029/2000JB000049.

Gök, R., et al. (2003), Shear wave splitting and mantle flow beneath LA RISTRA, *Geophys. Res. Lett.*, *30*(12), 1614, doi:10.1029/2002GL016616.

Granet, M., U. Achauer, and S. Sobolev (1988), Isotropic tomographic inversion and anisotropic mantle: What do we miss?, *Ann. Geophys.*, *16*(1), 154.

Hammond, W. C., and E. D. Humphreys (2000), Upper mantle seismic wave attenuation: Effects of realistic partial melt distribution, *J. Geophys. Res.*, *105*, 10,987–10,999.

Henstock, T. J., K. C. Miller, S. H. Harder, et al. (1998), Probing the Archean and Proterozoic lithosphere of western North America, *GSA Today*, *8*(7), 1–5.

Humphreys, E. D., K. G. Dueker, D. L. Schutt, et al. (2000), Beneath Yellowstone: Evaluating plume and nonplume models using teleseismic images of the upper mantle, *GSA Today*, *10*(12), 1–7.

Humphreys, E., E. Hessler, K. Dueker, et al. (2003), How laramie-age hydration of North American lithosphere by the Farallon slab controlled subsequent activity in the western United States, *Int. Geol. Rev.*, *45*, 575–595.

Karlstrom, K. E., and CDROM Working Group (2002), Structure and evolution of the lithosphere beneath the Rocky Mountains: Initial results from the CD-ROM experiment, *GSA Today*, *12*(3), 4–10.

Lange, R. A., I. S. E. Carmichael, and C. M. Hall (2000), 40Ar/39Ar chronology of the Leucite Hills, Wyoming: Eruption rates, erosion rates, and an evolving temperature structure of the underlying mantle, *Earth Planet. Sci. Lett.*, *174*(3–4), 329–340.

Leat, P. T., G. L. Hendry, and R. N. Thompson, et al. (1989), Quaternary volcanism in northwestern Colorado: Implications for the roles of asthenosphere and lithosphere in the genesis of continental basalts, *J. Volcanol. Geotherm. Res.*, *37*(3–4), 291–310.

Lee, D.-K., and S. P. Grand (1996), Upper mantle shear structure beneath the Colorado Rocky Mountains, *J. Geophys. Res.*, *101*, 22,233–22,244.

McKenzie, D. (1989), Some remarks on the movement of small melt fractions in the mantle, *Earth Planet. Sci. Lett.*, *95*(1–2), 53–72.

McMillan, M. E., C. L. Angevine, and P. L. Heller (2002), Postdepositional tilt of the Miocene-Pliocene Ogallala Group on the western Great Plains: Evidence of late Cenozoic uplift of the Rocky Mountains, *Geology*, *30*, 63–66.

Peng, X., and E. D. Humphreys (1998), Crustal velocity structure across the eastern Snake River Plain and the Yellowstone swell, *J. Geophys. Res.*, *103*, 7171–7186.

Sahagian, D., A. Proussevitch, and W. Carlson (2002), Timing of Colorado Plateau uplift: Initial constraints from vesicular basalt-derived paleoelevations, *Geology*, *30*, 807–810.

Saltzer, R. L., and E. D. Humphreys (1997), Upper mantle P wave velocity structure of the eastern Snake River Plain and its relationship to geodynamic models of the region, *J. Geophys. Res.*, *102*, 11,829–11,841.

Schmeling, H. (1985), Numerical models on the influence of partial melt on elastic, anelastic, and electric properties of rocks, *Phys. Earth Planet. Inter.*, *41*, 34–57.

Schott, B., D. A. Yuen, and H. Schmeling (2000), The diversity of tectonics from fluid-dynamical modeling of the lithosphere-mantle system, *Tectonophysics*, *322*(1–2), 35–51.

Schutt, D. L., and E. D. Humphreys (2004), *P* and *S* wave velocity and V_P/V_S in the wake of the Yellowstone hotspot, *J. Geophys. Res.*, *109*, B01305, doi:10.1029/2003JB002442.

Snelson, C. M., T. J. Henstock, G. R. Keller, et al. (1998), Crustal and uppermost mantle structure along the Deep Probe seismic profile, *Rocky Mountain Geol.*, *33*(2), 181–198.

Sobolev, S. V., U. Achauer, C. Bauer, et al. (1997), Upper mantle temperatures and lithosphere-asthenosphere system beneath the French Massif Central constrained by seismic, gravity, petrologic and thermal observations, *Tectonophysics*, *275*(1–3), 143–164.

Vandecar, J. C., and R. S. Crossen (1990), Determination of teleseismic relative phase velocity arrival times using multi-channel cross-correlation and least squares, *Bull. Seismol. Soc. Am.*, *80*(1), 150–169.

Yuan, H., and K. Dueker (2004), Upper mantle tomographic V_P and V_S images of the Rocky Mountains in Wyoming, Colorado, and New Mexico: Evidence for thick, laterally heterogeneous lithosphere, *Geophys. Monogr. Ser.*, AGU, Washington, D.C., in press.

Zurek, B., and K. Dueker (2004), Lithospheric layering beneath the southern Rocky Mountains from the CD-ROM experiment, *Geophys. Monogr. Ser.*, AGU, Washington, D.C., in press.

K. Dueker and H. Yuan, Department of Geology and Geophysics, University of Wyoming, 100 East University Avenue, Laramie, WY 82071-3006, USA. (dueker@uwyo.edu)